Optical imaging of multiphase coexistence in $Nd_{1/2}Sr_{1/2}MnO_3$

P. W. Kolb, D. B. Romero, and H. D. Drew
Laboratory for Physical Sciences, 8050 Greenmead Drive, College Park, Maryland 20740, USA

Y. Moritomo
Department of Applied Physics, Nagoya University, Nagoya 464-8603, Japan

A. B. Souchkov and S. B. Ogale
Department of Physics, University of Maryland, College Park, Maryland 20742, USA
(Received 23 June 2004; published 14 December 2004)

We report on the imaging of the coexistence of the *CE*-type charge-ordered insulator (COI) phase and the ferromagnetic metal (FMM) phase of $Nd_{1/2}Sr_{1/2}MnO_3$ by means of polarized optical microscopy over a range in temperature of several degrees. Consistent with the different Mn-O bond lengths along the *c* axis and in the *ab* plane, optical anisotropy is observed in the COI, FMM, and paramagnetic insulator phases. Upon cooling, accommodation strain leads to the rapid formation of martensiticlike COI *variants* within the FMM phase. Upon warming, the FMM phase is observed to nucleate slowly on COI variant boundaries where the magnitude of the strain is locally maximized. Consistent with the presence of strain, COI twin boundaries sometimes demonstrate optical anisotropy and can act as sites for FMM phase nucleation.

DOI: 10.1103/PhysRevB.70.224415 PACS number(s): 75.30.Kz

I. INTRODUCTION

An important characteristic of the pseudocubic manganites is a strong competition between several different thermodynamic phases. These include various types of charge ordered insulators (COIs) in some cases accompanied by spin order and e_g orbital ordering, a ferromagnetic metal (FMM), and a paramagnetic insulator (PM). The equilibrium phase at a particular temperature depends on the competition of the microscopic processes occurring on the manganese ions including the Jahn-Teller effect, double exchange, and on-site Coulomb repulsion. Because the interesting phase transitions occur in the solid state in these materials and generally involve the lattice degrees of freedom, they are usually accompanied by inhomogeneous strain. The presence of strain can affect the free energy of the phases and thereby the phase competition. The inhomogeneity of the strain leads to multiphase coexistence which has important consequences, such as the "colossal magneto resistance" phenomenon, and has received much recent attention.[1]

In this paper we report on the optical imaging of the electronic phases of $Nd_{1/2}Sr_{1/2}MnO_3$. The competing phases in this case are a low temperature, *CE*-type COI which is accompanied by spin order and e_g orbital ordering, a FMM with a transition temperature of about 160 K, and a PM with a transition temperature of about 250 K.[2] The transition from the COI phase to the FMM phase is first order and involves a change in crystal structure. The first-order nature is demonstrated by discontinuous changes in resistivity,[3] reflectance, magnetic susceptibility, and lattice constant. The crystal structure of $Nd_{1-x}Sr_xMnO_3$ is orthorhombic but can be understood as a distorted perovskite crystal. The octahedra formed by Mn atoms surrounded by six O atoms is apically compressed and tilted relative to the crystallographic axes. The distortions result in a pseudocubic lattice and differences of Mn-O bond lengths along the *c* axis and within the *ab* plane that increases from about 0.5% in the FMM and PM phases to about 1.1% in the COI phase for $Nd_{1/2}Sr_{1/2}MnO_3$.[2] Presumably, there are also differences in these bond lengths within the *ab* plane. As a result, the optical response for light polarized along each of the orthogonal crystal axes can be different. In principle this optical anisotropy can be exploited to observe domains of differing axis orientation within each electronic phase. These domains are referred to optical domains in this work to distinguish them from ferromagnetic domains or domains of different electronic phase. Since the difference of Mn-O bond lengths along the *c* axis and in the *ab* plane is about twice as large in the COI phase compared to the FMM or PM phases, contrast between optical domains in the COI phase are observed to be greater than in the FMM or PM phases.

Optical domains in metals have long been studied by polarization microscopy. The general technique of optical microscopy has been employed for some time to investigate many aspects of the microstructure of metals.[4] Included among these aspects is the formation of martensites[5] which has been recently suggested to be related to phase transitions in the manganites.[6] Martensitic transitions are characterized by the absence of diffusion of atoms, surface upheaval, and the generation of a large number of lattice imperfections such as stacking faults and internal twinning. Accommodation strain plays an important role in the formation of the martensite. For Fe-Ni alloys different *variants* or crystal orientations of the martensite phase form and grow in different places in the crystal, often penetrating other variants and deforming the twins found inside them.[5,7] For Fe-Ni alloys, there are 12 different possible variant orientations as worked out by Nishiyama.[5] In $Nd_{1/2}Sr_{1/2}MnO_3$, strain also plays an important role. In particular, uniform strain has been shown theoretically to stabilize the orbital ordering pattern of the half-doped manganites.[8] Accordingly, the inhomogeneity of accommodation strain should locally destabilize the COI

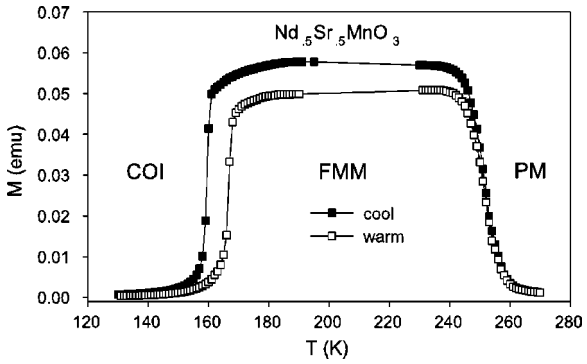

FIG. 1. Magnetic susceptibility of the $Nd_{1/2}Sr_{1/2}MnO_3$ sample. The poling field used is 0.2 Oe.

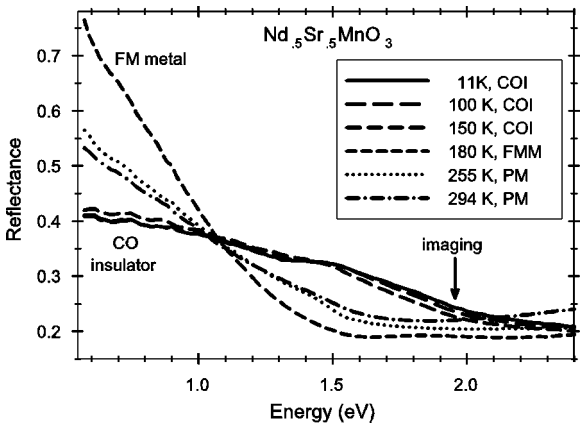

FIG. 2. Reflectance versus photon energy for $Nd_{1/2}Sr_{1/2}MnO_3$.

phase. The effects of the accommodation strain in the COI-to-FMM phase transition leads to an observable martensitic-like behavior with time dependent growth of needle-like phase domains and two phase coexistence over a substantial temperature range. Using optical microscopy we are able to image this transition and observe directly the nature of the nucleation and coexistence of the two phases.

II. SAMPLE CHARACTERIZATION AND PREPARATION

The $Nd_{1/2}Sr_{1/2}MnO_3$ sample studied in this work is single crystal grown by the floating zone method.[9] The sample was polished with a 9.8 pH, 0.05 μm silica suspension. The resulting surface was shown to be locally smooth but faceted by atomic force microscopy. The faceting was presumably due to differential polishing rates along different crystal axes. Following the recipe of H. J. Lee *et al.*, the sample was also annealed in an O_2 atmosphere at 1000 °C to remove surface damage.[10] The resulting surface was locally smoother but also demonstrated a higher density and complexity of faceting. The latter could be due to passage into and out of a rhomohedral phase during annealing. The existence of this additional phase is suggested by the phase diagram of the similar manganite $La_{1-x}Ca_xMnO_3$.[11] Some of the topography from the polishing/annealing process is "frozen-in" in the sense that it persists even as the surface undergoes upheaval during the FMM-COI phase transitions. These frozen-in features sometimes appear in optical micrographs and are not associated with optical domains.

Various measurements made on the sample show the first-order nature of the FMM-to-COI transition. Though no transport measurements have been made on this particular sample, the dc resistivity of similarly prepared samples are discontinuous near the FMM to COI transition.[3] In magnetic susceptibility measurements, as shown in Fig. 1, a clear FMM phase is observed, and the transition to the COI phase is hysteretic, a signature of a first-order transition. Measurements of the reflectance of the $Nd_{1/2}Sr_{1/2}MnO_3$ sample as a function of wavelength at different temperatures, shown in Fig. 2, also indicate a first-order COI to FMM phase transition. There is only a slight variation in the plot shape as temperature is raised from 11 to 150 K in the COI phase. However, at 180 K in the FMM phase, the plot shape discontinuously changes to a shape indicative of a metal with a high reflectance and a large slope at low photon energy. Suggestive of a *d-d* hopping transition in the COI phase changing to conduction of delocalized electrons in the FMM phase, oscillator strength around 1.5 eV in the COI phase is transferred to a Drude response at low energy in the FMM phase. Consequently, the COI reflectance in the visible and near infrared, used in the imaging experiments, is higher than the FMM reflectance.

III. IMAGING

A. Experimental setup

Micrographs of $Nd_{1/2}Sr_{1/2}MnO_3$ were taken with a traditional bright-field, reflection microscope. A tungsten lamp was used for illumination. A narrow-band interference filter (of bandwidth $\Delta\lambda$) was placed in the illumination path to make the light quasimonochromatic. The polarization was controlled by rotating a Glan-Taylor-type polarizer which was placed in the illumination path directly after the field aperture of the microscope. The sample was placed in an Oxford cryostat (Microstat) with a quartz optical window and was cooled by a continuous flow of liquid helium. A commercial heater and proportional integral derivative (PID) feedback circuit were used to control the sample temperature to within 0.1 K. Microscope objectives with magnifications (numerical apertures) of 10× (0.30) and 40× (0.55) were used. The 40× objective was designed to compensate for windows of varying thicknesses. Images were directed to the top of the microscope where they were recorded on a charge-coupled device camera. Typically, no analyzing polarizer was placed in front of the camera.

B. Optical anisotropy

Typical optical micrographs of the COI phase of $Nd_{1/2}Sr_{1/2}MnO_3$ reveal optical anisotropy and a large number of strain-induced lattice imperfections reminiscent of similar images of martensitic metals. Figure 3 shows the COI phase illuminated by different polarizations at low magnification. This particular region is dominated by two diagonal variants.

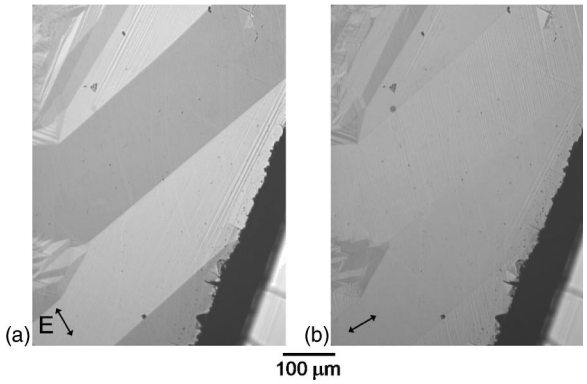

FIG. 3. Low magnification optical micrographs of the COI phase at 80 K using 600 nm ($\Delta\lambda = 25$ nm) illumination. The polarization (double arrows) is chosen for (a) large contrast between variants and (b) small contrast.

The variants appear as alternating bright and dark bands running from upper right to lower left. The micrographs of Fig. 4 at high magnification show that the variants are twinned.

As with polarization, changing the wavelength of illumination can reveal different features and provides evidence for the existence of strain on COI twin boundaries. This is shown in Fig. 5 where three wavelengths with two polarizations are used. For the polarization in Fig. 5(a), the contrast between twins is low. For the orthogonal polarization in Fig. 5(b), the contrast becomes large. Also present at all wavelengths and polarizations are faint bright lines at about 15° counterclockwise from the twins. These arise from the residual faceting of polishing/annealing and are essentially unchanged by wavelength or polarization. In Fig. 5(c) at 670 nm, the twins become bright on the upper edge and dark on the lower edge. This combination of wavelength and polarization is apparently sensitive to strain arising on the twin boundary. In this picture, stress causes the Mn-O bonds to change length and thus introduces additional optical anisotropy. The stress is likely tensile rather than shear, since this would produce the larger change in bond length; linear with tensile stress but quadratic for shear stress. Because the edges alternate between bright and dark, the stress also likely alternates from tensile, perpendicular to one side of the boundary, to compressive, perpendicular to the other side.

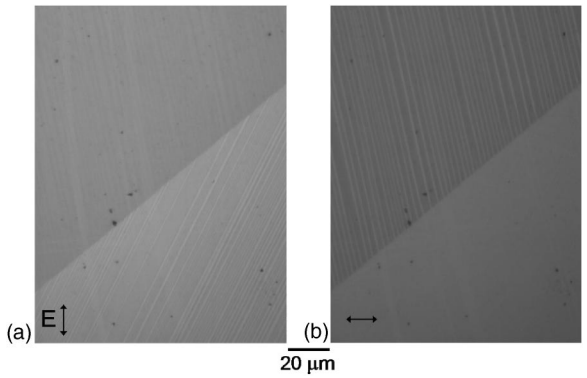

FIG. 4. High magnification optical micrographs of a COI variant boundary at 80 K using 600 nm ($\Delta\lambda = 25$ nm) illumination. The polarization (double arrows) is chosen to reveal twins in (a) the lower variant and (b) the upper variant.

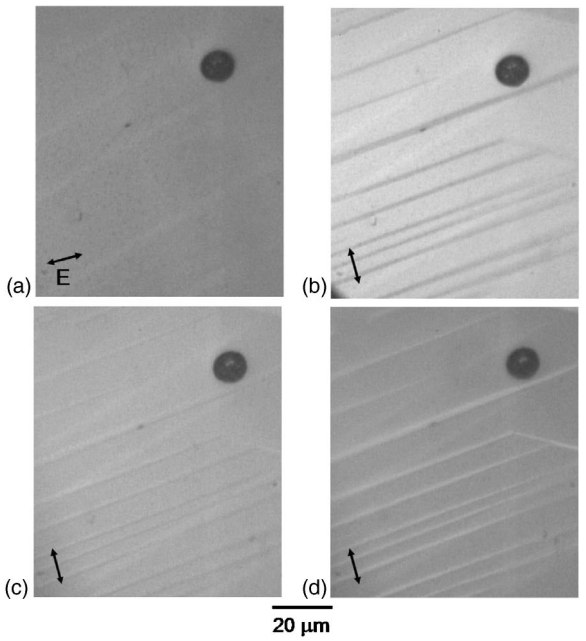

FIG. 5. Optical micrographs of COI twins at 80 K using (a) and (b) 630 nm, (c) 670 nm, and (d) 730 nm illumination ($\Delta\lambda = 10$ nm for all). The polarization (double arrows) is chosen for small contrast in (a) and for large contrast in (b)–(d).

Optical micrographs of the COI phase are similar to those in the FMM (see Figs. 6 and 7) and PM phase but differ in some fundamental ways. Contrast between optical domains

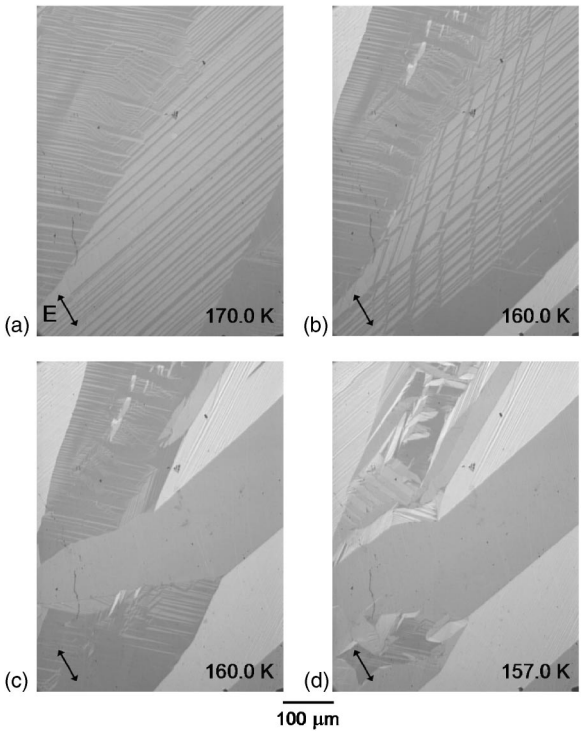

FIG. 6. Optical micrographs of the transition from FMM to COI using 600 nm light ($\Delta\lambda = 25$ nm) illumination.

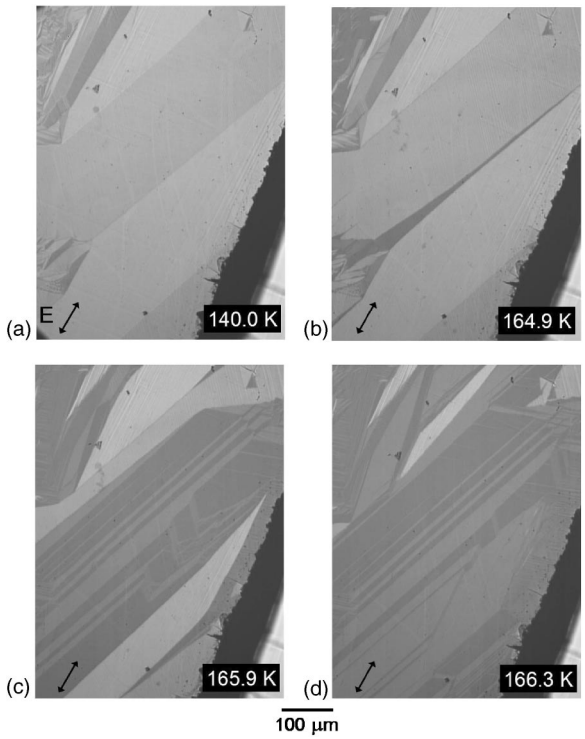

FIG. 7. Low magnification optical micrographs of the nucleation and growth of the FMM phase domains (dark regions) using 600 nm light ($\Delta\lambda = 25$ nm) illumination. The polarization (double arrows) is chosen to maximize contrast between FMM and COI phase domains.

in the COI phase is more pronounced than in the FMM phase. The overall image brightness is greater in the COI phase, as would be expected from the reflectance plots of Fig. 2. Upon cooling the sample into the FMM phase from the PM phase no obvious changes result. This is consistent with a transition primarily involving the electronic degrees of freedom rather than the crystal properties.

C. Formation of COI domains

The transition from FMM to COI was imaged as a function of temperature. Similar to a martensitic behavior, large COI phase domains appear suddenly as the temperature is lowered by just a few millidegrees Kelvin below the transition temperature. At constant temperature slightly below the transition temperature, some COI domains initially grow quickly, on a time scale of seconds, as large distinct variants. Growth then slows down to a crawl, and a drop in temperature of a few degrees is needed to complete the transition. Figure 6 shows one region as it undergoes a transition from FMM to COI. The situation depicted in Fig. 6(a) is unchanged until the temperature is reduced to about 160 K. At this point, wedges of bright COI variants slam through the top left and lower right regions of the micrograph as shown in Fig. 6(b). This has a dramatic effect on the FMM twins in the center as they become strained and distorted. Small, bright COI domains pop up in the upper part of the region. As shown in Fig. 6(c) at the same temperature, a slightly darker COI variant then penetrates the region from the middle right and joins the bright variant below it. The variants continue to grow as a large, bright variant appears in the upper right. Small, bright variants continue to pop up in other places. However, at this point the transition slows considerably, and the temperature must be lowered several degrees to continue and eventually complete the process. In Fig. 66(d), the temperature has been lowered by 3 K, but some dark FMM domains still remain. Accordingly, there are an increasing number of small COI variants with complex boundary patterns.

D. Nucleation of the FMM phase

Upon warming, the nucleation of the FMM occurs at first very slowly with onset (termination) at about 155 K (168 K) and tends to occur on variant boundaries. Nucleation and growth of the FMM phase are shown in Fig. 7 at low magnification. These micrographs are dominated by COI variant bands running diagonally from the lower left to the upper right (as also shown in Fig. 2). Additionally, there are smaller, irregularly shaped variants which are more difficult to pick out. The FMM phase domains, generally seen as dark regions, first appear along various variant boundaries, preferentially choosing some over others. The FMM domains then grow forming wedgelike patterns that eventually merge with other FMM domains. Qualitatively speaking, the initial FMM transition upon heating initially occurs much more slowly than the reverse transition, i.e., the COI growth upon cooling. The FMM nucleation on the variant boundary running through the center of Fig. 7 is shown under high mag-

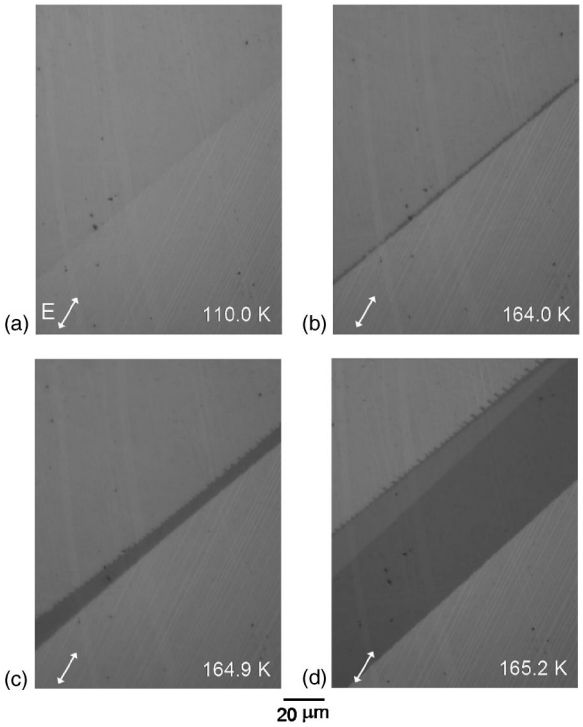

FIG. 8. High magnification optical micrographs of the nucleation and growth of the FMM phase domains using 600 nm ($\Delta\lambda = 25$ nm) illumination.

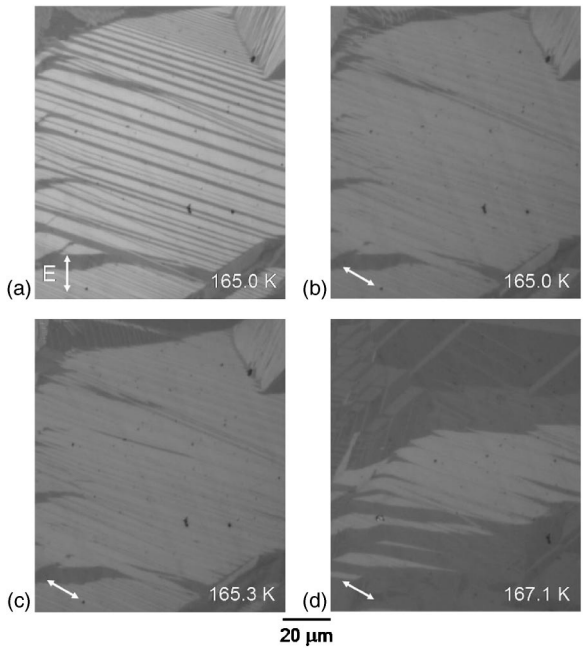

FIG. 9. Optical micrographs of the nucleation and growth of the FMM phase domains along COI twin using 600 nm ($\Delta\lambda = 25$ nm) illumination. The polarization (double arrows) is chosen (a) to reveal COI twins and (b)–(d) to cause FMM domains to appear dark and produce almost no contrast from COI twins.

nification in Fig. 8. These micrographs suggest that the FMM tends to nucleate where the magnitude of strain is at a maximum.

The FMM phase might also be expected to grow along twin boundaries due to a small amount of strain present on real twin boundaries. However, before this can occur, twinned COI regions are usually overwhelmed by FMM domains growing from elsewhere. What can be asserted from far-field imaging is that the FMM phase may occasionally nucleate on a twin boundary and often prefers to grow along a twin boundary than in a random location. An example of this is shown in Fig. 9. The polarization can be chosen to image the COI twin domain structure as in Fig. 9(a) or to pick out FMM domains as in Figs. 9(b)–9(d). As the temperature rises, a dark FMM needle appears roughly in the center of Fig. 9(c). Using the speck of dirt at its center as a fudicial mark, a comparison of Figs. 9(a) with 9(c) shows that the left part of the FMM needle lies along a COI twin boundary. The right part of the needle curves upward and terminates on another twin boundary. The needle then disappears at slightly higher temperature. As the temperature rises further, long narrow FMM wedges grow along the twin boundaries, shown in Fig. 9(d). Relative to the thinner COI twins, the FMM wedges point to the left on the upper boundaries and to the right on the lower boundaries.

IV. SUMMARY

Optical and phase domains of $Nd_{1/2}Sr_{1/2}MnO_3$ have successfully been imaged using polarized optical microscopy. Phase coexistence of COI and FMM phase domains has been observed over a range of 15 K. The phase transition is observed to be driven by inhomogeneous strain. In particular, the FMM phase is observed to nucleate upon warming on COI variant and twin boundaries where the magnitude of strain is locally maximized.

ACKNOWLEDGMENT

This work was supported by the NSF-MRSEC program of the NSF Grant No. DMR-00-80008.

[1] N. Mathur and P. Littlewood, Phys. Today **56**, 25 (2003).
[2] R. Kajimoto, H. Yoshizawa, H. Kawano, H. Kuwahara, Y. Tokura, K. Ohoyama, and M. Ohashi, Phys. Rev. B **60**, 9506 (1999).
[3] J. H. Jung, H. J. Lee, T. W. Noh, E. J. Choi, Y. Moritomo, Y. J. Wang, and X. Wei, Phys. Rev. B **62**, 481 (2000).
[4] A. Tomer, *Structure of Metals Through Optical Microscopy* (ASM International, Materials Park, Ohio, 1991).
[5] Z. Nishiyama, *Martensitic Transformation*, edited by M. Fine, M. Meshii, and C. Wayman (Academic Press, New York, 1978), p. 23.
[6] V. Podzorov, B. G. Kim, V. Kiryukhin, M. E. Gershenson, and S.-W. Cheong, Phys. Rev. B **64**, 140406 (2001).
[7] T. Maki, S. Shimooka, T. Arimoto, and I. Tamura, Trans. Jpn. Inst. Met. **14**, 62 (1973).
[8] M. J. Calderon, A. J. Millis, and K. H. Ahn, Phys. Rev. B **68**, 100401 (2003).
[9] Y. Moritomo, H. Kuwahara, Y. Tomioka, and Y. Tokura, Phys. Rev. B **55**, 7549 (1997).
[10] H. J. Lee, J. H. Jung, Y. S. Lee, J. S. Ahn, T. W. Noh, K. H. Kim, and S.-W. Cheong, Phys. Rev. B **60**, 5251 (1999).
[11] P. Schiffer, A. P. Ramirez, W. Bao, and S.-W. Cheong, Phys. Rev. Lett. **75**, 3336 (1995).